BIOCHEMISTRY
including biophysical chemistry & molecular biology

Article

pubs.acs.org/biochemistry

Pif97, a von Willebrand and Peritrophin Biomineralization Protein, Organizes Mineral Nanoparticles and Creates Intracrystalline Nanochambers

Eric P. Chang[†] and John Spencer Evans*

Laboratory for Chemical Physics, Division of Basic Sciences and Center for Skeletal Biology, New York University, 345 East 24th Street, New York, New York 10010, United States

Supporting Information

ABSTRACT: The formation of the mollusk nacre layer involves the assembly and organization of mineral nanoparticles into fracture-toughened mesoscale-sized aragonite tablets that possess intracrystalline nanoporosities. At least one nacre protein family, known as the framework proteome, is strategically located as part of a macromolecular coating around each nacre tablet and is believed to participate in tablet formation. Here, we report new studies of a recombinant form (rPif97) of a unique Japanese pearl oyster (*Pinctada fucata*) nacre framework biomineralization protein, Pif97. This unique protein possesses both a von Willlebrand factor type A domain (vWA, F23−Y161) and a Peritrophin A chitin-binding domain (PAC, E234−D298). rPif97 self-associates or aggregates to form amorphous protein phases that organize both amorphous and single-crystal calcium carbonate nanoparticles *in vitro*. Further, in the presence of nucleating calcite crystals, rPif97 protein phases deposit onto these crystals and become occluded over time, forming nanochambers within the crystal interior. The formation of these mineral-modifying amorphous protein phases is linked to the presence of intrinsic disorder and amyloid-like cross-β-strand aggregation-prone regions, and three-dimensional modeling indicates that both the vWA and PAC domains are accessible for intermolecular interactions. Thus, the vWA- and PAC-containing Pif97 protein exhibits key functionalities that would allow its participation in mollusk nacre layer tablet assembly and porosity formation.

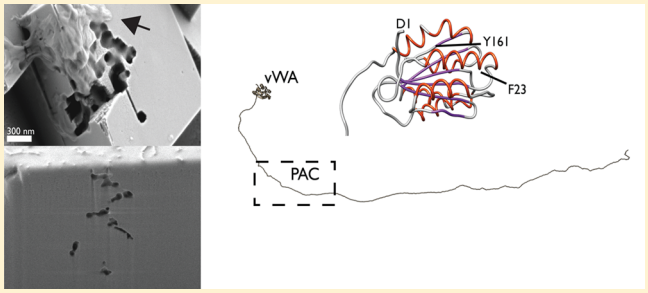

The mollusk shell nacre layer is an engineering marvel. This organic−inorganic composite structure consists of organized mesoscale single-crystal nanoporous aragonite tablets that are fracture resistant,[1−4] possess self-reparative capabilities,[5] and are assembled from mineral nanoparticle precursors.[6] The formation of the mollusk shell nacre layer is believed to be under the control of two protein families, the intracrystalline and the framework.[6,7] Of these, the framework proteome is the most unique, because these proteins associate with the macromolecular silk−β-chitin exterior gel-like phase that coats the exterior of the nacre tablets and is believed to be involved in the early stages of aragonite tablet formation.[8,9] Unfortunately, there is very little information available regarding this proteome and its participation in the nacre mineralization process. Thus, our present understanding of mollusk shell biomineralization is limited, and this in turn prevents us from understanding how proteins manage the nanoscale-to-mesoscale shell engineering process.

In the Japanese pearl oyster *Pinctada fucata*,[6,7] a framework proteome known as the Pif family exists.[10−17] One of these proteins, Pif97 (97 kDa, 525 amino acids, pI 4.65),[10−17] possesses two unique sequence features. The first is a Peritrophin A-type chitin polysaccharide-binding (PAC) domain[18,19] located at midsequence (E234−D298). This domain is believed to allow Pif97 to anchor to the β-chitin polysaccharide substrate within the framework layer.[13,16,17] The second is a von Willebrand factor type A domain (vWA) protein−protein interaction sequence[20−23] that is located at the N-terminus (F23−Y161).[10−17] This domain has been found in a number of nonbiomineralization proteins and functions as an adhesion, motility, or elastomeric domain.[20−23] Given that some nacre proteins assemble to form protein phases *in vitro* that order mineral nanoparticles and create nanoporosities within mineral crystals,[24−31] it is likely that the vWA- and PAC-containing Pif97 protein may function in a similar manner. If so, then this would add protein phase formation, mineral nanoparticle assembly, and intracrystalline modification to the functions with which vWA and PAC proteins are associated.[18−23]

We have discovered that the vWA- and PAC-containing Pif97 is indeed a self-associative nacre protein that organizes calcium carbonate mineral nanoparticles and creates nanoporosities within nucleating calcite crystals *in vitro*. Using an *Escherichia coli*-expressed recombinant version of the *P. fucata* Pif97 protein [designated as rPif97, 526 amino acids, sequence

Received: June 26, 2015
Published: August 10, 2015

DOI: 10.1021/acs.biochem.5b00842
Biochemistry 2015, 54, 5348−5355

G1−R526 (Figure S1 of the Supporting Information)], we found that rPif97 forms protein phases that consist of nanometer-sized amorphous-appearing protein complexes and films. Experimental studies confirm that the rPif97 sequence is intrinsically disordered, and bioinformatics indicates that the major region of disorder in the Pif97 protein is located in the C-terminal region (F162−R525), which also contains the putative PAC domain (E234−D298) and nine putative amyloid-like aggregation-prone cross-β-strand regions. Under *in vitro* mineralization conditions, rPif97 protein phases exhibit two unique traits. (a) They contain or are associated with either amorphous calcium carbonate (ACC) or single-crystal calcite mineral nanoparticles. (b) They randomly deposit onto exposed crystal surfaces, and as crystal overgrowth proceeds, these protein phases become entrapped and form intracrystalline nanochambers. Thus, the vWA- and PAC-containing framework protein Pif97 exhibits a structural and functional profile that can assist in the nanoscale-to-mesoscale engineering of the nacre layer.

EXPERIMENTAL PROCEDURES

Recombinant Expression and Purification of Pif97. The target DNA sequence of Pif97 (mature expressed form sans the membrane leader sequence) was taken from the Pif177 gene (Swiss-Prot entry C7G0B5.1, GenBank entry BAH97338.1), codon-optimized, chemically synthesized, and then inserted into the pUC57 vector. The cloning strategy included the incorporation at the N-terminus of the mature Pif97 sequence a Trx-His tag and a TEV cleavage site (Figure S1), and this combined sequence was subcloned into the expression vector E4 plasmid for *E. coli* expression as performed by GenScript USA (Piscataway, NJ) using their proprietary OptimumGene system.[24,26,28] An advantage of using the thioredoxin (Trx) tag in rPif97 expression is the antioxidant protection that Trx affords against unwanted oxidation of Cys thiol groups during expression and purification. *E. coli* BL21(DE3) was transformed with this recombinant plasmid, and a single colony was inoculated into LB medium containing kanamycin; cultures were incubated at 37 °C until the cell density reached an OD_{600} of 0.6−0.8, at which point IPTG was introduced for induction. A total of 20 L of bacterial culture was raised; cells were lysed by sonication, and the supernatant after centrifugation was loaded onto Ni-IDA resin columns for purification and eluted with gradient concentrations of imidazole. rPif97 protein was obtained from inclusion bodies with dialysis against TEV protease buffer and digestion with TEV protease. This digestion mixture was then again purified via Ni-IDA affinity chromatography, followed by Q-Sephasose ion exchange chromatography [linear gradient of 0 to 200 mM NaCl in 20 mM Tris-HCl (pH 7.5)] and Superdex 200 size exclusion chromatography [running buffer of 50 mM Tris-HCl (pH 8.0)]. After purification, the protein yield was 4 mg/20 L of culture and established as >90% pure by densitometric analysis of Coomassie Blue-stained sodium dodecyl sulfate−polyacrylamide gel electrophoresis 4 to 20% gradient gels (Figure S2). The purified protein was stored at −80 °C until it was needed.

Atomic Force Microscopy (AFM) Imaging of Pif97 Assemblies. We investigated the dimensional and morphological characteristics of rPif97 assemblies captured from solution onto mica substrates. The apo form (i.e., Ca^{2+}-free) of rPif97 was imaged in 10 mM Tris-HCl buffer (pH 8.0) at protein concentrations of 85, 170, 340, and 680 nM. In addition, we attempted to image rPif97 in 10 mM Tris-HCl and 10 mM $CaCl_2$ (pH 8.0) to mimic conditions similar to those found in our mineralization assays;[26,27,29,30] however, the introduction of Ca(II) ions led to extreme rPif97 aggregation that prevented AFM tip placement, and thus, we were unable to obtain useful images of rPif97 under pseudomineralization conditions. AFM experiments were conducted at 25 °C using an Agilent 5500 instrument operating in tapping mode in a buffer solution.[26,28,31] Olympus AC240TS rectangular-shaped, aluminum reflex-coated, silicon tips with a spring constant of approximately 2 N/m and a fluid drive frequency of ∼28 kHz were used for imaging. All samples were aliquoted onto a freshly stripped surface of mica (0.9 mm thick, Ted Pella, Inc.) and incubated for a period of 15 min at ambient temperature prior to measurement. Images were acquired at a scan rate of 2 Hz. Gwyddion software was implemented for image processing, noise filtering, and analysis, including the calculation of R_q, i.e., the surface roughness of the imaging surface.[26,28,31]

Calcium Carbonate Nucleation Studies. Stock concentrations of rPif97 were prepared using unbuffered deionized distilled water. Mineralization assays were adapted from published protocols[26,27,29−31] and were conducted by mixing equal volumes of 20 mM $CaCl_2{\cdot}2H_2O$ (pH 5.5) and 20 mM $NaHCO_3/Na_2CO_3$ buffer (pH 9.75) to a final volume of 500 μL in sealed polypropylene tubes and incubating at room temperature for 1 min, 5 min, 15 min, 30 min, and 1 h.[26,27,29−31] Aliquots of a rPif97 stock solution were added to the calcium solution prior to the beginning of the reaction, with final protein assay concentrations of 85, 170, 340, and 680 nM, identical to those utilized in AFM imaging experiments. The final pH of the reaction mixture was measured and found to be approximately 8.0−8.2.[26,27,29−31] Mineral and protein deposits formed during the assay were captured on 5 mm × 5 mm Si wafer chips (Ted Pella, Inc.) that were placed at the bottoms of the vials. Upon completion of the mineralization assay period, the Si wafers were rinsed thoroughly with calcium carbonate-saturated methanol and dried overnight at 37 °C prior to analysis. For TEM studies, a 10 μL aliquot of the mineralization assay supernatant was withdrawn at the completion of the assay period, spotted onto Formvar-coated Au TEM grids (Ted Pella, Inc.), and washed and dried as described above.

Electron Microscopy Imaging. Scanning electron microscopy (SEM) imaging of the Si wafers extracted from the mineralization assays was performed using a Merlin (Carl Zeiss) field emission SEM (FESEM) instrument using either an Everhart-Thornley type secondary electron detector (SE2) or an annular secondary electron detector (in lens) at an accelerating voltage of 1.5 kV, a working distance of 4 mm, and a probe current of 300 pA. Prior to analysis, SEM samples were coated with iridium using a Cressington 208HR sputter coater with a thickness controller attachment. Transmission electron microscopy (TEM) imaging and electron diffraction analyses were performed on Formvar-coated Au TEM grids containing dried supernatant samples using a Philips CM12 transmission electron microscope equipped with a tungsten filament electron beam source. All imaging and diffraction analyses were performed at 120 keV. A diffraction pattern of a polycrystalline gold standard was used as a calibration scale for all subsequently recorded diffraction patterns.[26,27,29,30] The selected area diffraction patterns were analyzed and indexed using ImageJ and the JEMS software package.

Focused Ion Beam (FIB) Sectioning and Imaging. Imaging of the internal crystal morphology was performed

DOI: 10.1021/acs.biochem.5b00842
Biochemistry 2015, 54, 5348−5355

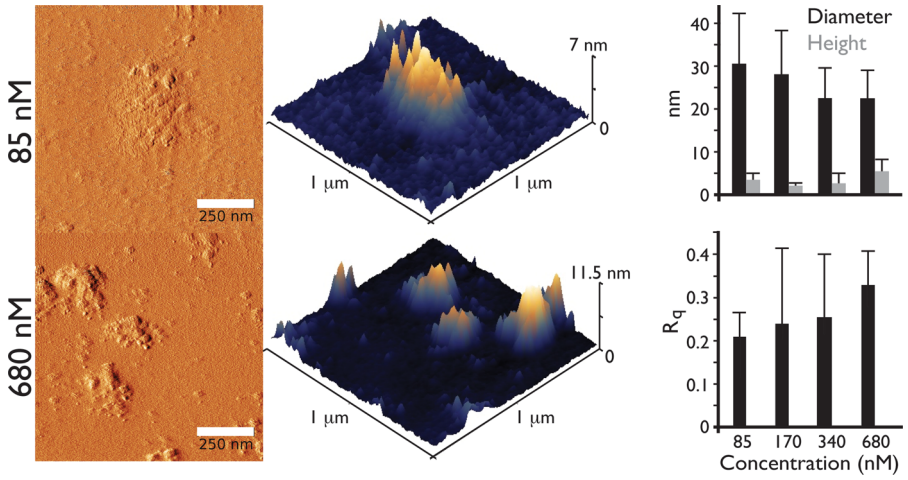

Figure 1. Concentration-dependent tapping mode AFM amplitude plots, height plots, and histogram distributions of mean particle diameters and heights for 85 and 680 nM rPif97 on freshly cleaved mica surfaces (pH 8.0) in 10 mM Tris-HCl. Note in the height plots that the rPif97 oligomers form a contiguous filmlike layer or coating on the mica surface. Histogram values represent measurements taken for 30 particles at each protein concentration.

using a Zeiss Auriga Small Dual-Beam FIB-SEM instrument.[29,30] For these analyses, all samples were first coated with 4 nm of iridium prior to SEM imaging and then coated with 50 nm of Au prior to the use of the FIB. A 30 kV, 120 pA gallium ion beam was oriented perpendicular to the sample by tilting the sample stage to 54° and utilized to mill 15 nm serial cross sections. SEM images of cross-sectioned surfaces were then obtained using a 2.0 kV, 600 pA electron beam and a secondary electron detector at a working distance of 5.0 mm. Images of surfaces containing electron beam damage were created for comparison to images of undamaged surfaces but were not used for the purposes of discussion in this publication. Images were taken shortly after cross sectioning to limit the exposure of the uncoated surfaces to the electron beam.[29,30]

Bioinformatics and Circular Dichroism (CD) Spectrometry. To determine a hypothetical global structure of Pif97, we utilized the DISOclust (version 1.1)-IntFOLD2 integrated protein structure and function prediction server (University of Reading, Reading, U.K., using default parameters), which provides tertiary structure prediction and three-dimensional (3D) modeling of protein sequences that contain folded and unfolded sequence elements.[32] CD spectra (190−260 nm) of 680 nM rPif97 in 10 mM Tris (pH 8.0) were recorded at 25 °C on the AVIV stopped flow 202SF CD spectropolarimeter. A total of eight scans per sample were collected in a cuvette with a path length of 0.1 cm, using a bandwidth of 1 nm, a wavelength step of 1 nm, and an averaging time of 0.5 s. The instrument was previously calibrated with *d*-10-camphorsulfonic acid. The recorded spectra were averaged and the appropriate background spectra (Tris buffer) subtracted. Spectra were smoothed using the binomial algorithm included in the AVIV CD software. Ellipticity is reported as mean residue ellipticity (degrees square centimeter per decimole). Secondary structure estimates of rPif97 samples were obtained using three different algorithms included in the CDPro software package (SELCON3, CDSSTR, and CONTILL) and the SMP56 Reference Protein Set.[33−35]

RESULTS

rPif97 Self-Associates To Form Disordered Protein Phases. A number of mollusk shell-associated proteins, including the n16 family, assemble or aggregate under low- and high-ionic strength conditions to form protein phases or hydrogels that modulate calcium carbonate nucleation.[26−31] Given the close association of n16.3 with Pif97,[10,11,16,17] we suspected that protein phase formation might also be common to Pif97. To determine this, we utilized tapping mode AFM imaging to monitor rPif97 aggregation on freshly cleaved mica surfaces [10 mM Tris-HCl (pH 8)]. As per previous studies, because of mineral particle formation and its intense effect on protein aggregation, we omitted Ca^{2+} and HCO_3^-/CO_3^{2-} ions from these imaging studies and simply mimicked the aqueous environment at the same pH.[26,27,29,30]

As shown in Figure 1, we observe the formation of amorphous-appearing supramolecular protein phases over a protein concentration range of 85−680 nM. Note that in the presence of 10 mM Ca^{2+}, these protein phases experience severe aggregation, such that AFM tip positioning is impractical (data not shown). This Ca^{2+}-mediated enhancement of self-association is also common to other nacre proteins.[26,27,29,30] In general, under low-ionic strength conditions, rPif97 protein phases appear to be comprised of multiple protein particles that have coalesced together. These phases are nanometer-sized and heterogeneous in dimension as evidenced by quantitative measurements extracted from the AFM images (Figure 1): we note approximately 30 and 50% variations in particle diameters and heights, respectively, over this protein concentration range. The contrast between surface roughness values (R_q) for a freshly cleaved mica surface in buffer (R_q = 0.078 nm) versus untreated mica surfaces exposed to rPif97 (R_q = 0.21−0.33 nm, an approximately 3−4-fold increase) confirms that rPif97, like other nacre-associated proteins, forms protein films on mica surfaces. From this, we conclude that rPif97 forms amorphous protein phases under low-ionic strength conditions, and in the presence of Ca^{2+}, the rate of this process increases dramatically, similar to the phenomena reported for the framework protein, n16.3.[26,27]

Effect of rPif97 Protein Phases on *in Vitro* Calcium Carbonate Nucleation. Next, we were interested in

DOI: 10.1021/acs.biochem.5b00842
Biochemistry 2015, 54, 5348−5355

determining the mineralization capabilities of rPif97 during *in vitro* calcium carbonate assays that predominantly generate calcite crystals. Although these assays do not promote aragonite formation, they do provide a controlled, time-resolved (<1 h) standardized, reproducible environment for comparative analyses of nacre-associated proteins under ambient conditions.[26,27,29−31] Using TEM, we examined deposits that were rescued from rPif97 and control assay supernatants as a function of time (Figures 2 and 3). Compared to protein-

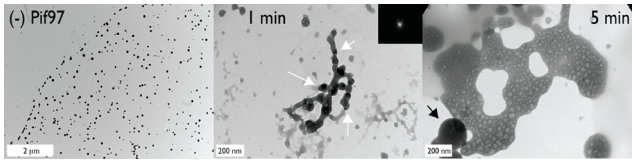

Figure 2. TEM images of supernatants taken from rPif97 assays (680 nM) at 1 and 5 min intervals. Arrows denote the presence of small electron-dense particles within the protein phase. The inset image for the 1 min deposit is the corresponding electron diffraction pattern obtained for the representative mineral deposit region within the protein phase. The (−) rPif97 image is of the supernatant from the 60 min (negative control) assay.

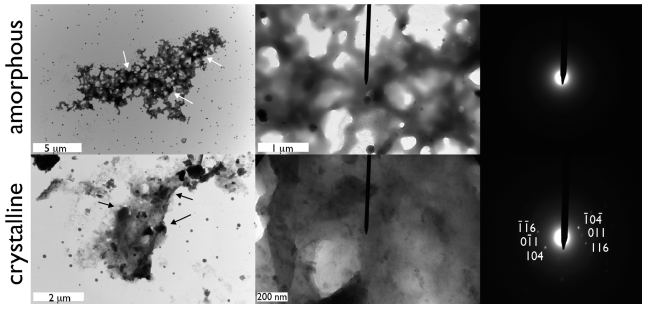

Figure 3. TEM images of supernatants taken from 680 nM rPif97 mineralization assays (60 min), revealing the presence of amorphous (ACC)- and crystalline (calcite)-containing protein−mineral complexes. Arrows denote locations of mineral deposits. Higher-magnification images of these protein−mineral deposits are presented along with corresponding electron diffraction patterns that are amorphous or index to single-crystal calcite.

deficient controls that generated only round amorphous-appearing mineral deposits, we detected rPif97 protein phases in the supernatants as early as 1 min. Although we were unable to directly document the effect of Ca^{2+} ions on rPif97 because of excessive aggregation during AFM, we do note that large, micrometer-sized protein phases are observed within mineralization environments (Figure 2), and we infer that Ca^{2+} environments promote additional rPif97 aggregation. These protein phases are often associated with electron-dense nanoscale round-to-irregular-shaped deposits. These dense deposits, which do not give rise to detectable electron diffraction patterns (Figure 2), are presumably ACC and appear to be entrapped within the protein phases. As time progresses, these protein phases approach the mesoscale and become denser, and by 60 min, we can distinguish two types of protein−mineral complexes, amorphous and crystalline (Figure 3). The amorphous complex features a protein network that possesses round nanoscale electron-dense deposits that do not yield an electron diffraction pattern (i.e., stabilized ACC deposits). In contrast, in the crystalline complex, we observe both round and angular electron-dense nanometer deposits. These angular deposits yield electron diffraction patterns corresponding to single crystal calcite (Figure 3).

Using these same assays, we also investigated the time-dependent formation of mineral deposits that precipitated onto Si wafer fragments (Figure 4, top panel). Once again, during

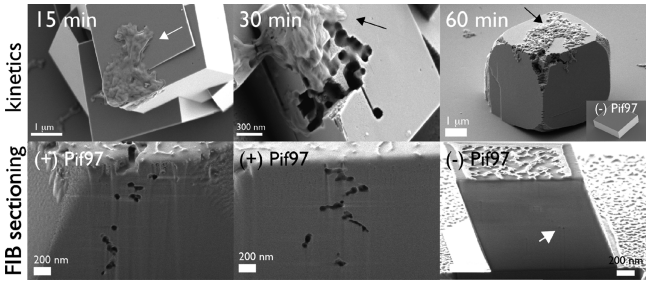

Figure 4. SEM images of mineral deposits (top row) captured on Si wafers from 680 nM rPif97 mineralization assays at 15, 30, and 60 min assay time points. Scale bars correspond to 10 μm. The inset image in the 60 min assay corresponds to calcite crystals obtained under (−) rPif97 (protein-deficient) assay conditions. SEM images of FIB-sectioned calcite crystals (bottom row, left and middle panels) taken from 680 nM rPif97 mineralization assays (60 min). In both images, one can clearly denote multiple intracrystalline porosities and chambers. The right panel in the bottom row shows the FIB section of a representative calcite crystal grown in (−) rPif97 mineralization assays, after 60 min (negative control).

the early stages of nucleation (1−15 min), we note the formation and deposition of protein phases within these assay systems, with the capture of these phases onto the Si wafers and formation of calcite crystals. At later time intervals (Figure 4, top panel, 30 min), we note that the protein phases have not significantly altered the calcite crystal morphologies relative to protein-deficient controls. What we do note is that the protein phases are becoming incorporated into the bulk crystal phase itself (i.e., intracrystalline incorporation) as mineralization proceeds. This incorporation process appears to be creating multichambered voids within the crystals. We confirmed this via focused ion beam (FIB) milling (Figure 4, bottom panel), where we discovered the presence of numerous intracrystalline nanoporosities, presumably representing the "footprints" of the incorporated rPif97 protein phases with these calcite crystals. The pores or voids created by rPif97 appear to be interconnected to one another, similar to the channels created by other intracrystalline nacre proteins within *in vitro* calcite crystals.[27,29,30] Eventually, as the assay progresses, we note that nanotexturing appears on calcite crystal surfaces, particularly at the edges, and it is evident that protein phase deposition is still ongoing and is most likely responsible for these surface changes (Figure 4, top panel, 60 min). This nanotexturing phenomenon reflects the ability of the protein phase to limit or inhibit calcite crystal growth.[27] From these observations, we conclude that rPif97 inhibits calcite crystal growth and becomes occluded within the forming calcite crystals over time.

Molecular Basis of Pif97 Assembly. The putative molecular features that allow Pif97 to form protein phases can be better understood using the DISOclust IntFOLD2 predicted 3D modeling prediction program, which uses sequence homology modeling to predict conformational preferences for both folded and unfolded regions (Figure 5).[32] Here, we observe the vWA fold (F23−Y161) as an accessible domain near the N-terminal portion of the protein.

DOI: 10.1021/acs.biochem.5b00842
Biochemistry 2015, 54, 5348−5355

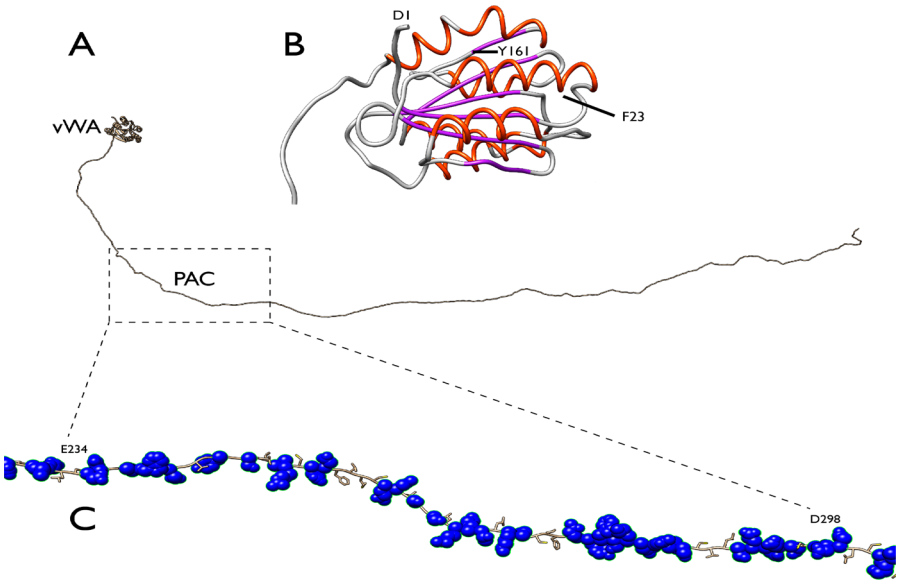

Figure 5. IntFOLD-predicted global structure of Pif97. The locations of the vWA and PAC domains are shown. For the vWA domain, secondary structures are denoted in color: red for α-helix, blue for β-sheet, and gray for random coil, loop, or turn regions. For the Pif97 PAC domain (D298−E234), polar side chains [i.e., anionic D and E, cationic K, R, and H, and hydrogen-bonding donor/acceptor S, T, N, Q, and Y) are presented in blue space-filling representations.

The top five models for this domain region had confidence and P value scores of 1.149×10^{-2} and global model quality scores of 0.4197, with the best fit to template crystal structure 1auqA (A1 domain of human von Willebrand factor).[36] We also note that the sequence region of F162−R525 downstream of the vWA domain possesses intrinsically disordered or unfolded regions (Figure S3 of the Supporting Information).[37−39] The presence of disordered regions was experimentally verified by circular dichroism (CD) spectrometry on aggregated apo-rPif97 protein samples (Figure 6). Here, we find that the CD spectra for rPif97 oligomers feature a strong (−) $\pi-$ π^* transition minimum band centered near 203 nm. By contrast, the published CD spectra for the vWA sequence[20,21] feature a broad (−) ellipticity band with minima at 208, 215, and 222 nm, which arise from multiple β-sheet−α-helix domains. Estimation of secondary structure preferences using reference data sets (CDSSTR, SELCON3, and CONTINLL)[33−35] reveals approximately 30−38% random coil, 24−29% β-turn, 12−20% regular β-strand, 6−9% distorted β-strand, 3−5% regular α-helix, and 5−13% distorted α-helix in rPif97 (inset of Figure 6). Thus, the CD spectra of rPif97 are consistent for a protein that is intrinsically disordered and possesses residual secondary structure regions.

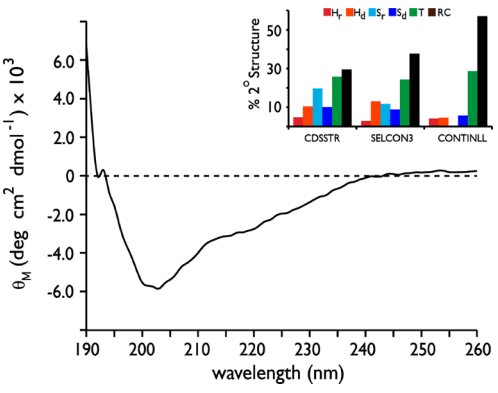

Figure 6. Circular dichroism spectra of 680 nM oligomeric rPif97 [10 mM Tris-HCl buffer (pH 8.0)]. The inset is a histogram plot of secondary structure content determined by CDPro (CDSSTR), SELCON3, and CONTINLL Reference Protein Sets. The histogram data are reported as the fractional weight distributed among regular helix (α_r), distorted helix (α_d), regular strand (β_r), distorted strand (β_d), turn (t), and random coil or unordered (rc) structures.

In addition to intrinsic disorder, the sequence region of F162−R525 is also notable for two other features. First, there are nine putative amyloid-like cross-β-strand aggregation-prone regions[40−42] that populate this sequence (Figure S3 of the Supporting Information). Presumably, these interactive regions may participate in the aggregation or protein phase formation process (Figure 1). Second, there is the presence of the putative chitin-binding domain, PAC [E234−D298 (Figure 5)].[18,19] This 64-amino acid polysaccharide-binding site is unfolded, and its amino acid content is 50% polar (13 anionic, 6 cationic, and 15 donor/acceptor residues). As noted in earlier studies of framework nacre polypeptide binding to β-chitin substrates,[43,44] polar amino acids would facilitate hydrogen bonding interactions with the carbohydrate -OH and -NH groups of β-chitin and allow Pif97 to stabilize to β-chitin surfaces within the silk-gel/polysaccharide outer coatings of the nacre tablets.[45,46] In conclusion, the interactive vWA and PAC domains, combined with significant levels of intrinsic disorder and aggregation-prone sequences, potentially create a highly reactive Pif97 protein molecule (Figures 1−4).

DISCUSSION

The mollusk shell nacre layer can be considered a proteomic-based material; i.e., the formation and maintenance of the inorganic mineral phase are dependent upon the time- and space-dependent expression of specialized protein families, such as intracrystalline and framework proteins.[6,7] In this report, we confirm that one *P. fucata* framework gene product, Pif97, forms disordered protein phases or aggregates that guide the mineralization process at both the early and later stages of crystal growth *in vitro*. We believe that disordered nacre protein

DOI: 10.1021/acs.biochem.5b00842
Biochemistry 2015, 54, 5348−5355

phase formation is linked to two key traits: (a) the presence of amyloid-like aggregation-prone cross-β-strand sequences[40−42] and (b) significant levels of intrinsic disorder or unfolded structure[37−39] (Figure S3 of the Supporting Information) that contribute to the instability and amorphous nature of protein phases that form in solution (Figures 1−4). During the early stages of nucleation, rPif97 forms mesoscale protein networks containing either ACC or crystalline calcite mineral nanoparticles (Figure 3). At this time, it is not clear whether the ACC mineral−protein complexes are predecessors to the calcite−protein complexes, or if both complexes represent dual end points in mineral nucleation and stabilization. Subsequently, during later stages of nucleation, rPif97 protein phases deposit onto existing crystal surfaces, and initially, these protein phases exhibit inert behavior. As a result, mineral overgrowth rapidly overcomes the protein phases and nanoporosities form in peripheral and central regions of the crystal (Figures 3 and 4). Over time, however, rPif does introduce nanotexturing to calcite crystal surfaces (Figure 3), and thus, this protein may possess calcite inhibition properties. Given that nacre tablets are formed from the assembly of calcium carbonate mineral nanoparticles[1,6] and proteins become occluded within the interior of the nacre tablets,[2,4] we extrapolate that the vWA- and PAC-containing Pif97 protein could play a major role in both phenomena with the nacre layer of *P. fucata*. Obviously, *in situ* experiments will be required to firmly establish this hypothesis.

The rPif97 data set presented here provides us with a unique opportunity to contrast this protein against the published data set obtained for its putative framework partner, n16.3.[24−27] With regard to the early stages of nucleation, both proteins are similar in that they form phases that organize amorphous and crystalline nanoparticles within the same assay periods (i.e., 5−15 min).[24−27] Where the differences emerge is in the later stages of the nucleation process, in particular, the formation and location of nanoporosities within calcite crystals. n16.3 protein phases rapidly introduce nanotexturing and directional change to growing crystal surfaces, which slows crystal growth, and subsequently, nanoporosities form only within the peripheral internal regions of the crystal.[24−27] In contrast, within the same time period, rPif97 protein phases do not immediately modify growing crystal surfaces; thus, mineral overgrowth rapidly overtakes the protein phase, and nanoporosities form in both the peripheral and central regions of nucleating crystals (Figures 3 and 4). We conclude that *P. fucata* Pif97 and n16.3 framework proteins perform similar mineral nanoparticle assembly and organization tasks but diverge with regard to modifications that are introduced into the exterior and interior regions of growing crystals. Further studies will be required to understand how these two proteins work together with Pif80 to create ordered aragonite mesocrystals in the nacre layer.

The participation of the PAC[18,19] and vWA[20−23] domains in numerous macromolecular interaction scenarios[13−15] indicates that these sequences are highly versatile for biological organisms, including those that form mineralized skeletal structures such as the pearl oyster. However, once Pif97 and its cohorts finalize nacre tablet assembly, we postulate that there may yet be another role for this protein. Given that the vWA domain is reported to be extensible and elastomeric[20−23] and that the β-chitin-containing framework layer that surrounds each nacre tablet exhibits an elastomeric response to force extension,[3,4] we foresee that the PAC- and vWA-containing Pif97 protein may anchor to β-chitin via the PAC domain and behave as an extensible species via the vWA domain. This would allow Pif97 not only to help with the nanoscale-to-mesoscale formation of the nacre tablets (Figures 2−4) but also to protect adjacent nacre tablets from catastrophic separation.[3,4] If true, then the evolutionary selection of the vWA and PAC domains for participation in pearl oyster shell nacre formation also enhanced the survivability of the nacre layer. An investigation into this scenario is currently in progress.

■ ASSOCIATED CONTENT

Supporting Information

The Supporting Information is available free of charge on the ACS Publications website at DOI: 10.1021/acs.biochem.5b00842.

Details of all mineralization assays, AFM imaging conditions, EM and FIB characterization methods, protein expression and preparation (Figures S1 and S2) and protocol and data for bioinformatics predictions of intrinsic disorder and amyloid-like cross-β-strand aggregation-prone sequences within Pif97 (Figure S3) (PDF)

■ AUTHOR INFORMATION

Corresponding Author

*Laboratory for Chemical Physics, Division of Basic Sciences and Center for Skeletal Biology, New York University College of Dentistry, 345 E. 24th St., New York, NY 10010. E-mail: jse1@nyu.edu. Telephone: (347) 753-1955. Fax: (212) 995-4087.

Present Address

[†]E.P.C.: Albert Einstein College of Medicine, Bronx, NY 10461.

Funding

This research was supported by the U.S. Department of Energy, Office of Basic Energy Sciences, Division of Materials Sciences and Engineering, under Award DE-FG02-03ER46099.

Notes

The authors declare no competing financial interest.

■ ACKNOWLEDGMENTS

We thank Dr. Iva Perovic for her assistance with the CD experiments. This report represents contribution 79 from the Laboratory for Chemical Physics, New York University.

■ ABBREVIATIONS

$TrxHis_6$, recombinant thioredoxin poly$(His)_6$ affinity tag; vWA, von Willebrand factor type A domain; PAC, Peritrophin A type chitin polysaccharide-binding domain; IPTG, isopropyl β-D-1-thiogalactopyranoside; TEV, tobacco etch virus nuclear inclusion endopeptidase; ACC, amorphous calcium carbonate; IDA, iminodiacetic acid; FIB, focused ion beam.

■ REFERENCES

(1) Zhang, G., and Li, X. (2012) Uncovering aragonite nanoparticle self-assembly in nacre − A natural armor. *Cryst. Growth Des. 12*, 4306−4310.

(2) Li, X., Chang, W. C., Chao, Y. J., Wang, R., and Chang, M. (2004) Nanoscale structural and mechanical characterization of a natural nanocomposite material: The shell of red abalone. *Nano Lett. 4*, 613−617.

(3) Smith, B. L., Schaffer, T. E., Viani, M., Thompson, J. B., Frederick, N. A., Kindt, J., Belcher, A., Stucky, G. D., and Morse, D. E. (1999) Molecular mechanistic origin of the toughness natural adhesives, fibres, and composites. *Nature 399*, 761−763.

DOI: 10.1021/acs.biochem.5b00842
Biochemistry 2015, 54, 5348−5355

(4) Sun, J., and Bhushan, B. (2012) Hierarchical structure and mechanical properties of nacre: A review. *RSC Adv. 2*, 7617−7632.
(5) Su, X. W., Zhang, D. M., and Heuer, A. H. (2004) Tissue regeneration in the shell of the giant queen conch, Strombus gigas. *Chem. Mater. 16*, 581−593.
(6) Li, X., and Huang, Z. (2009) Unveiling the formation mechanism of pseudo-single-crystal aragonite platelets in nacre. *Phys. Rev. Lett. 102*, 075502−075506.
(7) Zhang, G., and Xu, J. (2013) From colloidal nanoparticles to a single crystal: New insights into the formation of nacre's aragonite tablets. *J. Struct. Biol. 182*, 36−43.
(8) Bezares, J., Asaro, R. J., and Hawley, M. (2010) Macromolecular structure of the organic framework of nacre in Haliotis rufescens: Implications for mechanical response. *J. Struct. Biol. 170*, 484−500.
(9) Checa, A. G., Cartwright, J. H. E., and Willinger, M. G. (2011) Mineral bridges in nacre. *J. Struct. Biol. 176*, 330−339.
(10) Zhang, G., et al. (2012) The oyster genome reveals stress adaptation and complexity of shell formation. *Nature 490*, 49−54.
(11) Fang, D., Xu, G., Hu, Y., Pan, C., Xie, L., and Zhang, R. (2011) Identification of genes directly involved in shell formation and their functions in pearl oyster, Pinctada fucata. *PLoS One 6*, e21860.
(12) Kinoshita, S., Wang, N., Inoue, H., Maeyama, K., Okamoto, K., Nagai, K., Kondo, H., Hirono, I., Asakawa, S., and Watabe, S. (2011) Deep sequencing of ESTs from nacreous and prismatic layer producing tissues and a screen for novel shell formation-related genes in the pearl oyster. *PLoS One 6*, e21238.
(13) Suzuki, M., Saruwatari, K., Kogure, T., Yamamoto, Y., Nishimura, T., Kato, T., and Nagasawa, H. (2009) An acidic matrix protein, Pif, is a key macromolecule for nacre formation. *Science 325*, 1388−1390.
(14) Gardner, L. D., Mills, D., Wiegand, A., Leavesley, D., and Elizur, A. (2011) Spatial analysis of biomineralization associated gene expression from the mantle organ of the pearl oyster, Pinctada maxima. *BMC Genomics 12*, 455−470.
(15) Xiang, L., Su, J., Zheng, G., Liang, J., Zhang, G., Wang, H., Xie, L., and Zhang, R. (2013) Patterns of expression in the matrix proteins responsible for nucleation and growth of aragonite crystals in flat pearls of Pinctada fucata. *PLoS One 8*, e66564.
(16) Wang, X., Song, X., Wang, T., Zhu, Q., Miao, G., Chen, Y., Fang, X., Que, H., and Zhang, G. (2013) Evolution and functional analysis of the Pif97 gene of the Pacific oyster Crassostrea gigas. *Cur. Zool. 59*, 109−115.
(17) Suzuki, M., Iwashima, A., Kimura, M., Kogure, T., and Nagasawa, H. (2013) The molecular evolution of the Pif family proteins in various species of mollusks. *Mar. Biotechnol. 15*, 145−158.
(18) Du, X. J., Wang, J. X., Liu, N., Zhao, X. F., Li, F. H., and Xiang, J. H. (2006) Identification and molecular characterization of a peritrophin-like protein from fleshy prawn (Fenneropenaeus chinensis). *Mol. Immunol. 43*, 1633−1644.
(19) Jasrapuria, S., Arakane, Y., Osman, G., Kramer, K. J., Beeman, R. W., and Muthukrishnan, S. (2010) Genes encoding proteins with peritrophin A-type chitin-binding domains in *Tribolium castaneum* are grouped into three distinct families based on phylogeny, expression and function. *Insect Biochem. Mol. Biol. 40*, 214−227.
(20) Zhang, W., Deng, W., Zhou, L., Xu, Y., Yang, W., Liang, X., Wang, Y., Kulman, J. D., Zhang, X. F., and Li, R. (2015) Identification of a juxtamembrane mechanosensitive domain in the platelet mechanosensor glycoprotein Ib-IX complex. *Blood 125*, 562−569.
(21) Luken, B. M., Winn, L. Y. N., Emsley, J., Lane, D. A., and Crawley, J. T. B. (2010) The importance of vicinal cysteins, C1669 and C1670, for von Willebrand factor A2 domain function. *Blood 115*, 4910−4913.
(22) Beckmann, A., Xiao, S., Muller, J. P., Mercadante, D., Nuchter, T., Kroger, N., Langhojer, F., Petrich, W., Holstein, T. W., Benoit, M., Grater, F., and Ozbek, S. (2015) A fast recoiling silk-like elastomer facilitates nanosecond nematocyst discharge. *BMC Biol. 13*, 3.
(23) Song, G., Koksal, A. C., Lu, C., and Springer, T. A. (2012) Shape change in the receptor for gliding motility in Plasmodium sporozoites. *Proc. Natl. Acad. Sci. U. S. A. 109*, 21420−21425.
(24) Ponce, C. B., and Evans, J. S. (2011) Polymorph crystal selection by n16, an intrinsically disordered nacre framework protein. *Cryst. Growth Des. 11*, 4690−4696.
(25) Evans, J. S. (2013) Liquid-like" biomineralization protein assemblies: A key to the regulation of non-classical nucleation. *CrystEngComm 15*, 8388−8394.
(26) Perovic, I., Chang, E. P., Lui, M., Rao, A., Cölfen, H., and Evans, J. S. (2014) A framework nacre protein, n16.3, self-assembles to form protein oligomers that participate in the post-nucleation spatial organization of mineral deposits. *Biochemistry 53*, 2739−2748.
(27) Chang, E. P., Russ, J. A., Verch, A., Kröger, R., Estroff, L. A., and Evans, J. S. (2014) Engineering of crystal surfaces and subsurfaces by framework biomineralization protein phases. *CrystEngComm 16*, 7406−7409.
(28) Perovic, I., Mandal, T., and Evans, J. S. (2013) A pearl protein self-assembles to form protein complexes that amplify mineralization. *Biochemistry 52*, 5696−5703.
(29) Chang, E. P., Williamson, G., and Evans, J. S. (2015) Focused ion beam tomography reveals the presence of micro-, meso-, and macroporous intracrystalline regions introduced into calcite crystals by the gastropod nacre protein AP7. *Cryst. Growth Des. 15*, 1577−1582.
(30) Chang, E. P., Russ, J. A., Verch, A., Kröger, R., Estroff, L. A., and Evans, J. S. (2014) Engineering of crystal surfaces and subsurfaces by an intracrystalline biomineralization protein. *Biochemistry 53*, 4317−4319.
(31) Perovic, I., Chang, E. P., Verch, A., Rao, A., Cölfen, H., Kröger, R., and Evans, J. S. (2014) An oligomeric C-RING nacre protein influences pre-nucleation events and organizes mineral nanoparticles. *Biochemistry 53*, 7259−7268.
(32) Roche, D. B., Buenavista, M. T., Tetchner, S. J., and McGuffin, L. J. (2011) The IntFOLD server: an integrated web resource for protein fold recognition, 3D model quality assessment, intrinsic disorder prediction, domain prediction and ligand binding site prediction. *Nucleic Acids Res. 39*, W171−176.
(33) Sreerama, N., and Woody, R. W. (2000) Estimation of protein secondary structure from circular dichroism spectra: Comparison of CONTIN, SELCON, and CDSSTR methods with an expanded reference set. *Anal. Biochem. 287*, 252−260.
(34) Lobley, A., Whitmore, L., and Wallace, B. A. (2002) DICHROWEB: An interactive website for the analysis of protein secondary structure from circular dichroism spectra. *Bioinformatics 18*, 211−212.
(35) Sreerama, N., and Woody, R. W. (2004) On the analysis of membrane protein circular dichroism spectra. *Protein Sci. 13*, 100−112.
(36) Emsley, J., Cruz, M., Handin, R., and Liddington, R. (1998) Crystal structure of the von Willebrand Factor A1 domain. Implications for the binding of platelet glycoprotein 1b. *J. Biol. Chem. 273*, 10396−10401.
(37) Tompa, P. (2002) Intrinsically unstructured proteins. *Trends Biochem. Sci. 27*, 527−533.
(38) Meng, J., Romero, P., Yang, J. Y., Chen, J. W., Vacic, V., Obradovic, Z., and Uversky, V. N. (2008) The unfoldomics decade: An update on intrinsically disordered proteins. *BMC Genomics 9*, S1−S26.
(39) Peysselon, F., Xue, B., Uversky, V. N., and Ricard-Blum, S. (2011) Intrinsic disorder of the extracellular matrix. *Mol. BioSyst. 7*, 3353−3365.
(40) Linding, R., Russell, R. B., Neduva, V., and Gibson, T. J. (2004) A comparative study of the relationship between protein structure and beta-aggregation in globular and intrinsically disordered proteins (TANGO). *J. Mol. Biol. 342*, 345−353.
(41) Conchillo-Sole, O., de Groot, N. S., Aviles, F. X., Vendrell, J., Daura, X., and Ventura, S. (2007) AGGRESCAN: a server for the prediction and evaluation of "hot spots" of aggregation in polypeptides. *BMC Bioinf. 8*, 65−82.
(42) Goldschmidt, L., Teng, P. K., Riek, R., and Eisenberg, D. (2010) The amylome, all proteins capable of forming amyloid-like fibrils. *Proc. Natl. Acad. Sci. U. S. A. 107*, 3487−3492.

DOI: 10.1021/acs.biochem.5b00842
Biochemistry 2015, 54, 5348−5355

(43) Keene, E. C., Evans, J. S., and Estroff, L. A. (2010) Matrix interactions in biomineralization: Aragonite nucleation by an intrinsically disordered nacre polypeptide, n16N, associated with a β-chitin substrate. *Cryst. Growth Des. 10*, 1383−1389.
(44) Keene, E. C., Evans, J. S., and Estroff, L. A. (2010) Silk fibroin hydrogels coupled with the n16N - beta-chitin complex: An in vitro organic matrix for controlling calcium carbonate mineralization. *Cryst. Growth Des. 10*, 5169−5175.
(45) Levi-Kalisman, Y., Falini, G., Addadi, L., and Weiner, S. (2001) Structure of the nacreous organic matrix of a bivalve mollusk shell examined in the hydrated state using cryo-TEM. *J. Struct. Biol. 135*, 8−17.
(46) Nudelman, F., Shimoni, E., Klein, E., Rousseau, M., Bourrat, X., Lopez, E., Addadi, L., and Weiner, S. (2008) Forming nacreous layer of the shells of the bivalves Atrina rigida and Pinctada margaritifera: An environmental- and cryo-scanning electron microscopy study. *J. Struct. Biol. 162*, 290−300.

DOI: 10.1021/acs.biochem.5b00842
Biochemistry 2015, 54, 5348−5355